LiMo8O10: Polar Crystal Structure with Infinite Edge-Sharing Molybdenum Octahedra

Zachary Messegee, Philippe Gall, Hari Bhandari, Peter Siegfried, Chang-Jong Kang, Benjamin Chen, Carl Conti, Banghao Chen, Mark Croft, Qiang Zhang, et al.

Inorganic Chemistry

pubs.acs.org/IC Article

$LiMo_8O_{10}$: Polar Crystal Structure with Infinite Edge-Sharing Molybdenum Octahedra

Zachary T. Messegee,[†] Philippe Gall,[†] Hari Bhandari, Peter E. Siegfried, Chang-Jong Kang, Benjamin Chen, Carl R. Conti, III, Banghao Chen, Mark Croft, Qiang Zhang, Syed N. Qadri, Joseph Prestigiacomo, Nirmal J. Ghimire, Patrick Gougeon,* and Xiaoyan Tan*

Cite This: https://doi.org/10.1021/acs.inorgchem.2c01917 Read Online

ACCESS | Metrics & More | Article Recommendations | Supporting Information

ABSTRACT: Polycrystalline $LiMo_8O_{10}$ was prepared in a sealed Mo crucible at 1380 °C for 48 h using the conventional high-temperature solid-state method. The polar tetragonal crystal structure (space group $I4_1md$) is confirmed based on the Rietveld refinement of powder neutron diffraction and $^7Li/^6Li$ solid-state NMR. The crystal structure features infinite chains of Mo_4O_5 (i.e., $Mo_2Mo_{4/2}O_{6/2}O_{6/3}$) as a repeat unit containing edge-sharing Mo_6 octahedra with strong Mo−Mo metal bonding along the chain. X-ray absorption near-edge spectroscopy of the Mo-L_3 edge is consistent with the formal Mo valence/configuration. Magnetic measurements reveal that $LiMo_8O_{10}$ is paramagnetic down to 1.8 K. Temperature-dependent resistivity [ρ(T)] measurement indicates a semiconducting behavior that can be fitted with Mott's variable range hopping conduction mechanism in the temperature range of 215 and 45 K. The ρ(T) curve exhibits an exponential increase below 5 K with a large ratio of $\rho_{1.8}/\rho_{300}$ = 435. $LiMo_8O_{10}$ shows a negative field-dependent magnetoresistance between 2 and 25 K. Heat capacity measurement fitted with the modified Debye model yields the Debye temperature of 365 K.

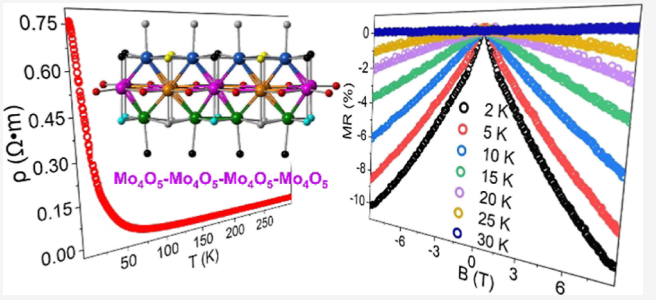

INTRODUCTION

Ternary alkali metal molybdenum oxides (also known as molybdenum bronzes), $A_xMo_yO_z$ (A = Li, Na, K, Rb, and Cs), are a fascinating family with unique and complex crystal structure features and exhibit exotic physical properties. For example, quasi-2D purple bronzes $A_{0.9}Mo_6O_{17}$ (A = Li, Na, and K) with layers of corner-sharing MoO_6 octahedra and MoO_4 tetrahedra exhibit anisotropic resistivity (e.g., 0.003 and 0.21 Ω•cm at room temperature along with the plate axis and perpendicularly to that axis in $Na_{0.9}Mo_6O_{17}$).[1] $Na_{0.9}Mo_6O_{17}$ and $K_{0.9}Mo_6O_{17}$ show metallic behavior from room temperature to 88 and 120 K, respectively, at which charge density wave-like transition occurs.[1] Quasi-1D (infinite chains of corner-sharing MoO_6 octahedra) blue bronzes $A_{0.3}MoO_3$ (A = K, and Rb; space group $C2/m$) exhibit a similar metal-to-insulator/semiconductor Peierls transition.[2] $Li_{0.9}Mo_6O_{17}$ ($P2_1/m$) exhibits quasi-1D metallic behavior and an interesting exponential increase in resistivity between ~24 and 2 K (a possible metal-to-insulator transition related to dimensional crossover), attains a superconducting state below 1.8 K, and manifests a large magnetoresistance just above the superconducting transition temperature.[3,4]

In addition to the quasi-1D/2D corner-sharing octahedral (MoO_6) and tetrahedral (MoO_4) chains in $A_{0.9}Mo_6O_{17}$ (A = Li, Na, and K) compounds, there is yet another interesting structural feature in ternary/quaternary molybdenum oxides. They have infinite chains of Mo_4O_y cluster units containing condensed edge-sharing Mo_6 octahedra with Mo−Mo metal bonding. Reported examples include AMo_4O_6 (A = Na, K, In, and Sn; space group $P4/mbm$),[5−8] $Sc_{0.75}Zn_{1.25}Mo_4O_7$ (space group $Imam$), isostructural $Ti_{0.5}Zn_{1.5}Mo_4O_7$,[9] $GaMgMo_4O_7$, $Fe_2Mo_4O_7$,[10] AMo_8O_{10} (A = Li, Zn; space group $I4_1md$),[11] $R_4Mo_4O_{11}$ (R = Y, Nd, and Sm-Tm; space group $Pbam$),[12] and $Mn_{1.5}Mo_8O_{11}$ (space group $P2_1/a$ and $P2_1/n$).[13,14] The metallic behavior in AMo_4O_6 (A = Na and In) and $Mn_{1.5}Mo_8O_{11}$[9,14,15] and the metal-to-insulator transition in AMo_4O_6 (A = K and Sn),[8,16,17] have been attributed to the infinite Mo−Mo bonding chains in the crystal structure. Among these reported compounds, AMo_4O_6 (A = Na and K) and $LiMo_8O_{10}$ belong to ternary alkali metal molybdenum oxides, and $LiMo_8O_{10}$ is the only one that adopts a polar space group. $LiMo_8O_{10}$ crystallizes with the tetragonal crystal structure in space group $I4_1md$, featuring infinite chains of Mo_4O_5 repeating units containing edge-sharing Mo_6 octahedra that extend along the tetragonal a and b axes (Figure 1).[11,18] f1

Received: June 2, 2022

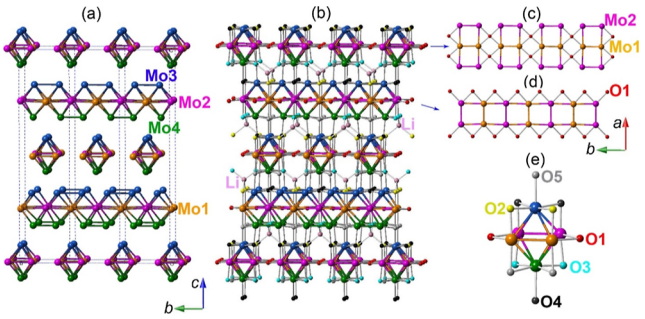

Figure 1. Projected view of the Mo connection (a), crystal structure of $LiMo_8O_{10}$ along the a axis (b), corresponding Mo1−O1−Mo2 connection in the *ab* plane (c) and (d), and "Mo_6O_{12}" cluster unit (f).

Strong Mo−Mo bonding along the chains is likely to give rise to a metallic behavior. As the polarity and metallic behavior are reported only in a few oxides,[19] the possible metallic behavior of $LiMo_8O_{10}$ makes it a prime candidate for a rare and interesting polar metallic oxide yet to be studied. Another exciting feature of $LiMo_8O_{10}$ is the low valence state of Mo due to the high concentration of Mo in the formula unit.[11] Up to now, the valence state of Mo and the physical properties of this compound remain unknown.

To investigate the physical properties and elucidate the nature of electrical conductivity of $LiMo_8O_{10}$ as a candidate for polar metallic oxides, we prepared polycrystalline $LiMo_8O_{10}$ samples with the high-temperature solid-state method. We used neutron powder diffraction data to refine the crystal structure; X-ray absorption near-edge spectroscopy (XANES) to reveal the valence state of Mo; and performed a detailed study of the magnetic, electrical, and thermal properties. We also performed the first-principle density functional theory calculations to study the electronic structure.

EXPERIMENTAL SECTION

Starting Materials and Synthesis. Polycrystalline $LiMo_8O_{10}$ samples were prepared by the solid-state reaction at high temperature with the starting reagents Li_2MoO_4, MoO_3, and Mo, all in powder form. The precursor Li_2MoO_4 molybdate was synthesized by heating the mixture of MoO_3 (99.95% mass fraction, CERAC) and Li_2CO_3 (99.9% mass fraction, CERAC) with an equal molar ratio in an alumina crucible at 600 °C in air for 12 h. MoO_3 and Li_2CO_3 were used as received. Mo powder (99.9% mass fraction, CERAC) was additionally purified by heating under a flow of hydrogen gas at 1000 °C for 6 h. The stoichiometric mixture of Li_2MoO_4, MoO_3, and Mo was finely ground; pressed into a pellet (about 4 g); and finally loaded into a molybdenum crucible, which was previously degassed at about 1500 °C for 15 min under a dynamic vacuum (~10^{-5} Torr). The molybdenum crucible was then sealed under low argon pressure using a homemade arc-welding system. The sealed crucible was heated in a graphite resistance furnace at a heating rate of 300 °C/h up to 1380 °C and was maintained at the same temperature for 48 h. The sealed crucible was then cooled at a rate of 100 °C/h down to 1100 °C, at which the furnace was turned off and allowed to cool to room temperature. A dense pellet (diameter = 3 mm) was prepared for physical properties measurements by pressing prepared polycrystalline powders at 400 °C for 6 h under 4 GPa with a Walker-type high-pressure instrument.

X-ray and Neutron Powder Diffraction. The X-ray powder diffraction analyses for the prepared Li_2MoO_4 and $LiMo_8O_{10}$ samples were performed using a D8 Bruker Advance diffractometer equipped with a LynxEye detector (Cu Ka_1) operating at 40 kV and 40 mA. The X-ray powder diffraction of the final product shows that the predominant phase is $LiMo_8O_{10}$, with MoO_2 and Mo as small impurities (Figure S1). Neutron powder diffraction (NPD) data were collected at 300 K using the Powder Diffractometer POWGEN at the Spallation Neutron Source,[20] Oak Ridge National Laboratory. A neutron band with a center wavelength of 0.8 Å high-resolution setting was used to collect the data with a broad *d* coverage of 0.16−7.5 Å. Rietveld refinements of the NPD data were carried out with the suite of FullProf programs.[21]

Chemical Analysis. Elemental analysis of polycrystalline $LiMo_8O_{10}$ sample was performed with a JEOL scanning electron microscopy (SEM), JSM-IT500HRLV SEM, with the accessory of Octane Elect Plus energy-dispersive X-ray (EDX) spectroscopy system and AOPEX Advanced software. The SEM images were collected with an accelerating voltage of 15 kV.

X-ray Absorption Near-Edge Spectroscopy. The Mo-L_3 edge XANES of $LiMo_8O_{10}$ were collected at beamline 7-ID-2 SST-2 using a Si-111 monochromator at the National Synchrotron Light Source II (NSLS-II), Brookhaven National Laboratory. The measurements were performed in the total electron yield mode. Measurements were made with MoO_3 and Li_2MoO_4 simultaneous standards for precision energy calibration. Standard polynomial background and postedge normalization to unity were used in the analysis.

Solid-State ^{7}Li and ^{6}Li NMR. The ^{7}Li and ^{6}Li magic-angle spinning (MAS) NMR spectra of polycrystalline $LiMo_8O_{10}$, LiCl, and Li_2O were measured at 298 and 238 K on a Bruker 500WB AVIII HD solid-state NMR spectrometer (11.74 T) equipped with 2.5 mm HXY and 4 mm HXY Bruker probes. A single-pulse experiment and spin-echo pulse sequences were applied with 90 pulses of 3.0 and 4.5 μs and MAS spinning speeds of 25 and 14 kHz for the 2.5 and 4 mm probes, respectively. The operating Larmor frequencies of ^{6}Li and ^{7}Li were 73.63 MHz and 194.45 MHz, respectively. A recycle delay time of 10−30 s was used. The chemical shift was referenced to LiCl(s) at −1.1 ppm with respect to aqueous LiCl.

Physical Properties. Magnetic susceptibility measurements were performed on a polycrystalline $LiMo_8O_{10}$ sample with a quantum design superconducting quantum interference device MPMS magnetometer. Field-cooled (FC) protocol was used to measure magnetic susceptibility between 1.8 and 300 K with the external magnetic field (B) of 0.1 T. The electrical resistivity and heat capacity were measured on two separate pieces of the same dense pellet (density > 91%) using a quantum design dynacool physical property measurement system. A four-probe method was used to measure resistivity and magnetoresistance by attaching 25 μm Pt wires using Epotek H20E silver epoxy. Isothermal magnetoresistance data were collected between 2 and 30 K using *B* up to ± 9 T. Magnetoresistance data were symmetrized about $B = 0$ T to account for the small misalignment of the voltage leads.

First-Principle Calculations. The first principle calculations were carried out with the all-electron full-potential linearized augmented plane-wave method implemented in the WIEN2k software package.[22] The experimental crystal structure was adopted for the calculations. The calculations were set up using the generalized gradient approximation with the on-site Coulomb repulsion U for 5 eV at Mo d orbitals.

RESULTS AND DISCUSSION

Synthesis and the Crystal Structure. The preparation of $LiMo_8O_{10}$ adopts the high-temperature solid-state method with similar conditions used in the previous report.[18] The X-ray powder diffraction analysis of the prepared sample indicates a successful synthesis of the primary phase $LiMo_8O_{10}$ with additional small impurities of MoO_2 and Mo present (Figure S1). The obtained phase is consistent with the reported tetragonal crystal structure with the polar space group $I4_1md$.t

In the crystal structure, strong Mo−Mo covalent bonds form Mo_6 octahedra that contain two waist Mo1 and Mo2, and one apical Mo3 atom and one Mo4 atom. The Mo_6 octahedra are edge-shared via Mo1−Mo1 and Mo2−Mo2 bonds and form infinite chains along the *a* and *b* axis, respectively (Figure

https://doi.org/10.1021/acs.inorgchem.2c01917
Inorg. Chem. XXXX, XXX, XXX−XXX

1a,c,d). The infinite chains of cluster units provide channels for strong metal−metal bonding, which indicates the potential metallic behavior in $LiMo_8O_{10}$. The individual chains are linked by Mo1−O1−Mo2 bonds and form layers. The structure features layers of edge-sharing Mo_6 octahedra chains stacking along the crystallographic *c* axis. The parallel edge-sharing Mo_6 octahedra chain extends along the *a* axis in one layer and then rotates 90° (along the *b* axis) in the adjacent layer in a crosswise layout connected by the shared O4 and O5 atoms. The special layout of the Mo_6 octahedra chain in the crystal structure of $LiMo_8O_{10}$ is different from the parallel feature of the Mo_6 octahedra chain in AMo_4O_6 (A = Na, K, In, and Sn),[5−8] $Sc_{0.75}Zn_{1.25}Mo_4O_7$,[9] $R_4Mo_4O_{11}$,[12] and $Mn_{1.5}Mo_8O_{11}$.[13,14] The Mo_6 octahedra are coordinated with twelve O atoms above corners and free edges and form a "Mo_6O_{12}" cluster (Figure 1f). Considering the shared O and Mo atoms together, the connective formula is $Mo_2Mo_{4/2}O_{6/2}O_{6/3}$ (leading to a "Mo_4O_5" unit). Consequently, the cluster unit in chains could be described as two repeated Mo_4O_5 subunits in the formula $Li(Mo_4O_5)(Mo_4O_5)$. Li coordinates with four O (O2 and O3) atoms and locates between the channels between the layers and the Mo_4O_5 units, which connects all clusters as a whole crystal structure (Figure 1b).

Because neutrons are more sensitive to light elements (Li and O) than X-rays, we used NPD to refine the crystal structure. The NPD data were collected at room temperature, and Rietveld refinements of the NPD data (Figure 2) were

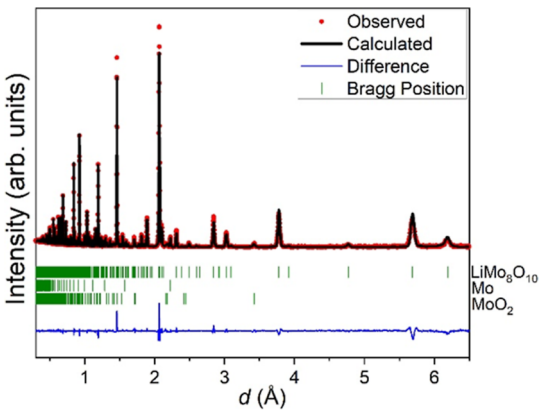

Figure 2. Rietveld refinement of NPD (300 K) of $LiMo_8O_{10}$ (space group $I4_1mb$) with observed data (red), calculated pattern (black), the difference between the observed and calculated patterns (blue), and Bragg peak positions (green) of $LiMo_8O_{10}$, Mo, and MoO_2.

carried out using the reported tetragonal crystal structure (space group $I4_1md$) as the starting model. The experimental NPD pattern can be fitted with the primary $LiMo_8O_{10}$ phase (mass % = 93.2%), a small amount of impurity Mo (mass % = 3.5%), and MoO_2 (mass % = 3.3%). Selected refined structural parameters of the major phase are given in Tables 1 and 2. The refined unit cell parameters are $a = b = 5.84503(5)$ Å, $c = 24.7558(3)$ Å, and $V = 845.77(1)$ Å^3, which are close to the reported values, $a = b = 5.8515(6)$ Å, $c = 24.783(3)$ Å, and $V = 848.6(2)$ Å^3.[4] The refined atomic positions are also close to the reported values.[4]

As shown in Figure 1e, each Mo_6 octahedra contains twelve Mo−Mo bonds, and the refined bond distance ranges from 2.678 to 2.925 Å (Table 2 and Figure 3). The averaged Mo−Mo bond distance is 2.81 Å, which is close to that (2.809 Å) of isostructural $ZnMo_8O_{10}$,[11] and other compounds (2.803 Å in

Table 1. Selected Structural Parameters of Rietveld Refinement of $LiMo_8O_{10}$

sample		$LiMo_8O_{10}$	
temperature		300 K	
mol wt, g/mol		934.62	
density (calculated),g/cm^3		7.339	
neutron source		T.O.F	
space group, #		$I4_1md$, # 109	
Z		4	
lattice parameters		$a = b = 5.84503(5)$ Å	
		$c = 24.7558(2)$ Å	
		$V = 845.77(1)$ Å3	
Rietveld criteria of fit[a]		$R_p = 4.57\%$, $R_{wp} = 3.56\%$, $R_F = 8.33\%$	
site	Wyckoff symbol	*x*, *y*, *z*	*B*
Li1	4a	0.5, 0.5, 0.126(2)	1.0(1)
Mo1	8b	0.5, 0.2291(5), 0	0.43(3)
Mo2	8b	0, 0.2344(6), 0.0044(1)	0.27(3)
Mo3	8b	0, 0.2445(6), 0.3293(2)	0.65(4)
Mo4	8b	0, 0.2746(5), 0.1765(2)	0.23(2)
O1	8b	0.5, 0.2434(8), 0.25	0.41(3)
O2	8b	0.5, 0.2427(7), 0.0822(3)	0.59(5)
O3	8b	0.5, 0.2374(8), 0.4235(2)	0.51(5)
O4	8b	0, 0.2530(9), 0.0895(3)	0.89(8)
O5	8b	0, 0.2707(8), 0.4168(3)	0.45(6)

Table 2. Selected Bond Distances in $LiMo_8O_{10}$

Mo−Mo distances (Å)		**Mo−O/Li−O** distances (Å)	
Mo1−Mo1	2.678 (4)	Mo1−O1 (×2)	2.129(4)
Mo1−Mo2 (×2)	2.925(1)	Mo1−O2	2.036(7)
Mo1−Mo3 (×2)	2.773(4)	Mo1−O5	2.059(7)
Mo1−Mo4 (×2)	2.770(4)	Mo2−O1 (×2)	2.161(4)
Mo2−Mo2	2.740(5)	Mo2−O3	2.009(6)
Mo2−Mo3 (×2)	2.747(5)	Mo2−O4	2.110(8)
Mo2−Mo4 (×2)	2.707(5)	Mo3−O2 (×2)	2.015(4)
Mo3−Mo3	2.858(5)	Mo3−O4 (×2)	2.117(5)
Mo3−Mo3	2.987(5)	Mo3−O5	2.172(9)
Mo4−Mo4	2.636(4)	Mo4−O3 (×2)	2.025(4)
Mo4−Mo4	3.209(4)	Mo4−O4	2.158(9)
Mo3−Mo4 (×4)[a]	3.256(6)	Mo4−O5 (×2)	2.104(4)
Mo1−Mo1[a]	3.167(4)	Li−O3 (×2)	1.82(3)
Mo2−Mo2[a]	3.105(5)	Li−O2 (×2)	1.85(3)

[a]Interchain distance.

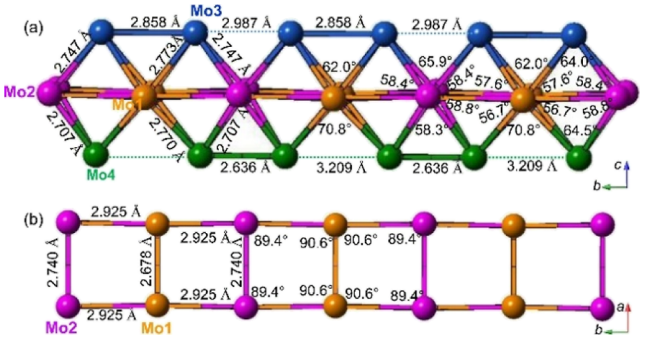

Figure 3. Mo−Mo bond distances and angles within the Mo_6 octahedra chain in the *bc* (a) and *ab* planes (b).

https://doi.org/10.1021/acs.inorgchem.2c01917
Inorg. Chem. XXXX, XXX, XXX−XXX

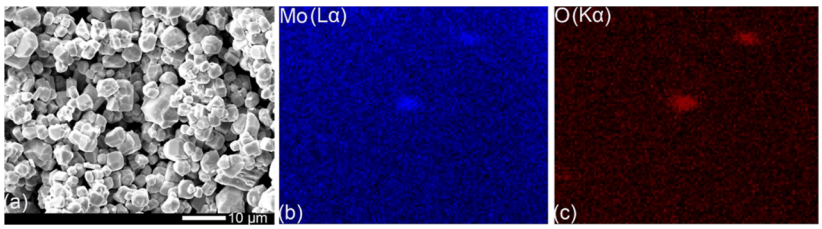

Figure 4. SEM image (a) and EDX mapping of Mo (b) and O elements (c) of $LiMo_8O_{10}$ particles.

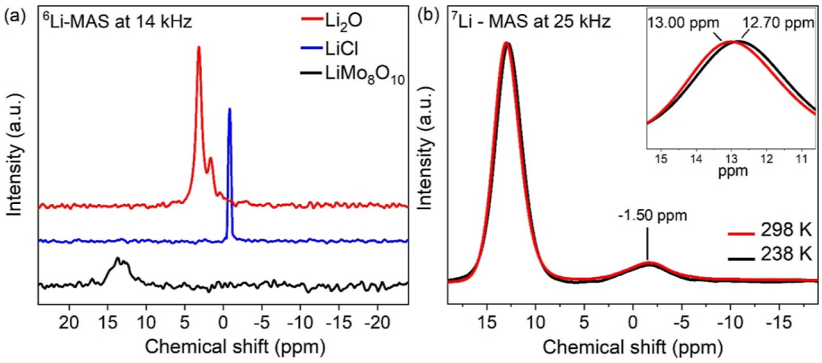

Figure 5. (a) ^{6}Li MAS NMR at 298 K and (b) ^{7}Li-MAS NMR of $LiMo_8O_{10}$ at 298 and 238 K.

$NaMo_4O_6$,[18] 2.799 Å in $Sc_{0.75}Zn_{1.25}Mo_4O_7$,[9] 2.790 Å in $Mn_{1.5}Mo_8O_{11}$,[18] and 2.80 Å in $R_4Mo_4O_{11}$[12]) containing the infinite edge-sharing Mo_6 octahedra. Because of the seven different Mo−Mo bond distances (Mo1−Mo1, Mo1−Mo2, Mo1−Mo3, Mo1−Mo4, Mo2−Mo2, Mo2−Mo3, and Mo2−Mo4), the Mo_6 octahedra is highly distorted. In the Mo_6 octahedra, the bond distances between waist Mo1 and Mo2 atoms are different (Mo1−Mo1 = 2.678 Å, Mo2−Mo2 = 2.740 Å, and Mo1−Mo2 = 2.925 Å), and the angles of Mo2−Mo2−Mo1 and Mo1−Mo2−Mo2 are 89.4 and 90.6°, respectively (Figure 3b). Inside the chain, each Mo_6 octahedra is connected by two Mo_6 octahedra via trans-edge-sharing Mo1−Mo1 and Mo2−Mo2 bonds on both sides with different tilting angles, so the chain (with a slightly tilted basal plane) can be viewed as a repeated unit of two edge-sharing Mo_6 octahedra.

Because of the distorted Mo_6 octahedra and the noncentrosymmetric distribution of Mo_6 octahedra, this compound adopts a polar crystal structure, which is different from other centrosymmetric compounds featuring chains of edge-sharing Mo_6 octahedra.[18] The two edge-sharing tilted Mo_6 octahedra result in alternate short and long Mo−Mo distances between the apical Mo3 (Mo3−Mo3 = 2.858, 2.987 Å) and Mo4 (Mo4−Mo4 = 2.636, 3.209 Å) atoms of two neighboring octahedra along the chain (Figure 3a). The long Mo−Mo distances are nonbonding, resulting in short alternated Mo3−Mo3 (2.858 Å) and Mo4−Mo4 (2.636 Å) bonds that connect Mo_6 octahedra within the chain. This pairwise distortion between apical Mo atoms is also observed in isostructural $ZnMo_8O_{10}$,[11] $R_4Mo_4O_{11}$,[12] $Mn_{1.5}Mo_8O_{11}$,[13] and $Sc_{0.75}Zn_{1.25}Mo_4O_7$[9] compounds featuring infinite chains of edge-sharing Mo_6 octahedra. One exception is the AMo_4O_6 (A = Na, K, In, and Sn; space group $P4/mbm$) crystal structure,[5−8] which contains undistorted chains of Mo_4O_6 units.

Considering all O atoms connected to Mo_6 octahedra, the infinite chains can be viewed as a repeated unit of two Mo_4O_5 clusters. The refined twelve Mo−O bond distances range from 2.009 to 2.16 Å (Table 2), which are close to the Mo−O bond distances (2.01−2.067 Å) in $NaMo_4O_6$,[5] and other Mo-containing compounds which contains edge-sharing Mo_6 octahedra in the crystal structure.[9,12,18] The bond strength (s) expressed in the valence unit of Mo−O can be calculated according to the equation $s(Mo-O) = [d(Mo-O)/1.882]^{-6}$,[23,24] where 1.882 Å is the Mo−O single bond distance, and the exponential parameter −6 corresponds to the value characteristic of the Mo atom. Based on the Mo−O bond distances, s(Mo−O) can be calculated for each Mo atom, and the bond valence sum (ν) of each Mo atom can be derived using the equation, $\nu = \Sigma s(Mo-O)$. The calculated ν are 2.16, 2.05, 2.74, and 2.75 (average 2.43) for Mo1, Mo2, Mo3, and Mo4, respectively. The metal-centered electrons (MCE) that are available for Mo−Mo bonding per Mo_4 unit are calculated to be 14.3 e^- (4 × 6−2.16−2.05−2.74−2.75) based on the ν of Mo atoms, which is close to the MCE value of 14.5 e^- [4 × 6−4×(10 × 2−1 × 1)/8] according to the formula $LiMo_8O_{10}$. Previous summary and analysis of similar compounds predicted that the distortion occurred due to electrons occupying antibonding bands in crystal structures with MCE > 13 e^-.[25,26] This is also the case in $LiMo_8O_{10}$, where strong distortion is shown in the cluster. Higher MCE values also cause additional distortion to the structure. The distorted Mo_6 octahedra in $LiMo_8O_{10}$ are very similar to that in the $R_4Mo_4O_{11}$ (R = Y, Nd, and Sm-Tm),[12] but $LiMo_8O_{10}$ contains two pairs of short/long apical Mo−Mo bonding along the chain, while $R_4Mo_4O_{11}$ only includes one pair, which makes the $LiMo_8O_{10}$ more distorted. From the perspective of MCE values, the calculated MCE (14.3 e^-) of $LiMo_8O_{10}$ is larger than that of $R_4Mo_4O_{11}$ (13.9−14.1 e^-),[12] suggesting a more distorted crystal structure as well.

Chemical Analysis. The prepared polycrystalline sample was examined by the SEM−EDX measurement. The SEM images indicate the particles to be polyhedral in shape and less than 10 μm in size (Figure 4a). Elemental mapping on the surface of polyhedrons confirms the Mo and O elements in the structure, but Li is too light to be detected using this technique (Figure 4b,c). Overall, the Mo and O elements are

https://doi.org/10.1021/acs.inorgchem.2c01917
Inorg. Chem. XXXX, XXX, XXX−XXX

homogeneously distributed through the polyhedron with two small areas with different concentrations, which probably correspond to the small amount of impurity seen as white dots on the polyhedron in the SEM image (Figure 4a). The obtained molar ratio of the Mo/O ratio is 8.0:9.6, which supports the expected ratio of 8:10 according to the formula $LiMo_8O_{10}$.

Solid-State ^{7}Li and ^{6}Li NMR. To confirm the existence of Li elements and study the local coordination environment of Li atoms in the crystal structure, solid-state ^{7}Li and ^{6}Li NMR were conducted using LiCl and Li_2O as the reference compounds. Both ^{7}Li and ^{6}Li MAS NMR spectra collected at room temperature show obvious peaks at 13.00 and 12.99 ppm, respectively (Figure 5). The ^{7}Li NMR spectrum shows broader peaks than that of ^{6}Li due to larger quadrupolar interaction. The ^{6}Li NMR spectra are dominated by chemical shift effects, which make them potentially more useful for providing structural information because their chemical shift more closely approximates the isotropic chemical shift.

Comparing the coordination environment of Li in the crystal structure of the LiCl and Li_2O references, Li atoms are located in the octahedral site within LiCl, while Li atoms occupy both the octahedral and tetrahedral sites within Li_2O. The systematic decrease observed in the ^{6}Li chemical shift from $LiMo_8O_{10}$ to Li_2O and LiCl corresponds with an increasing coordination environment that resulted from increased shielding, which can be described by a linear relationship.[27] The ^{6}Li chemical shift of $LiMo_8O_{10}$ indicates the tetrahedral environment of Li atoms, as shown in the crystal structure Figure 1b. To check the Li mobility, we also collected ^{7}Li MAS NMR spectra at 238 K. In comparison to the main resonance at 13.00 ppm obtained at 298 K, a sharper peak occurs at 12.70 ppm at 238 K. The main resonance shift indicates the change of distribution under a similar coordination environment. The broadening effect of resonances at a higher temperature suggests wider distribution due to higher mobility.

X-ray Absorption Near-Edge Spectroscopy. Figure 6 shows XANES measurements of the Mo-L_3 edges of $LiMo_8O_{10}$ and a series of oxide standards with differing valances/configurations: MoO_3 (Mo^{6+}, d^0), $SrFe_{0.5}Mo_{0.5}O_3$ (Mo^{5+}, d^1), $Sm_2Mo_2O_7$ (Mo^{4+}, d^2), MoO_2 (Mo^{4+}, d^2), and elemental Mo (Mo^0, d^5). The intense near-edge "white line" (WL) features in the spectra are due to dipole transitions from the 2p core level into empty 4d final states.[28−32] The characteristic chemical shift of the absorption edge to higher energy with increasing valence can be seen in Figure 6 by the systematic shift to the higher energy of the centrum of the WL feature with increasing Mo-valence.[28−34] The loss of screening (an increase of binding energy) with increasing valence is typically invoked for such chemical shift trends.[34] The strong splitting of the oxide spectra due to ligand field and band structure effects can complicate the evaluation of the WL chemical shift.[28−32] The first moment of the near edge, E_M, as defined in eq 1, has been used to estimate the relative chemical shifts of XANES spectra with strong spectral features.[32,33] In applying this method to estimate the relative WL chemical shifts of the spectra shown in Figure 6, the low energy integration limit, E_L = 2516 eV (well below the edge) was used. Following the analysis performed in the Re-containing compounds,[32] the high energy limit was chosen as the energy where the postedge absorption coefficient fell below the absorption coefficient of μ = 1.5 (Figure 6).

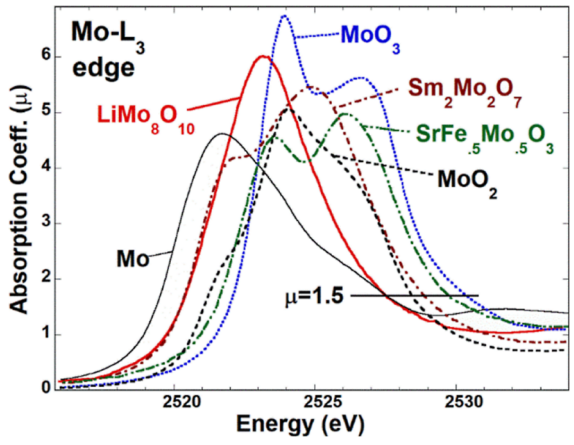

Figure 6. The Mo-L_3 near edges of $LiMo_8O_{10}$ and a series of standard Mo-containing compounds. The horizontal line at μ = 1.5 indicates the cutoff energy for integrating the first moment (E_M) of the WL feature to estimate the valence/configuration chemical shift.

$$E_M = \left[\int_{E_L}^{E_H} E\mu(E)\mathrm{d}E\right]\left[\int_{E_L}^{E_H} \mu(E)\mathrm{d}E\right]^{-1} \quad (1)$$

In Figure 7, the WL-feature moments for all of the spectra are plotted versus their formal 4d-counts and fitted to a straight

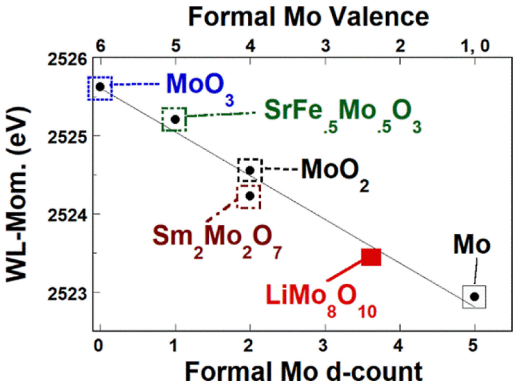

Figure 7. The Mo-L_3 edge WL chemical, as estimated by the first moment WL energies, plotted vs the formal Mo *d*-count (lower scale) and the formal valence (upper scale). The solid line is a linear fit to all of the data as a test of consistency.

line. There are two points that should be noted. First, the d-count dominance in the chemical shift has been tacitly assumed because the $4d^5$ configuration is common to both Mo^0 ($4d^5\ 5s^1$) and Mo^+ ($4d^5\ 5s^0$). This assumption is partially justified by the quadratic chemical shift versus valence relation found in some theoretical and experimental treatments of the Mo-shift, which flattens in the sub-Mo^{2+} range.[31] Second, due to the shortage of Mo^{2+} and Mo^{1+} standards, the formal $LiMo_8O_{10}$ configuration of $Mo^{2.375+}$ ($4d^{3.625}$) was included in the linear fit. With these caveats, the observed chemical shift of $LiMo_8O_{10}$ can be viewed to be consistent with its formally expected valence/configuration. Although such consistency is encouraging, the Mo−Mo bonding would be expected to play a strong role in this material, requiring considerations well beyond formal valence.

Physical Properties. Magnetic properties were investigated on a $LiMo_8O_{10}$ powder sample. Temperature-dependent FC magnetic susceptibility (χ) data were collected between

https://doi.org/10.1021/acs.inorgchem.2c01917
Inorg. Chem. XXXX, XXX, XXX−XXX

1.8 and 300 K (Figure 8), which indicates that $LiMo_8O_{10}$ is paramagnetic in this temperature range. Inverse susceptibility

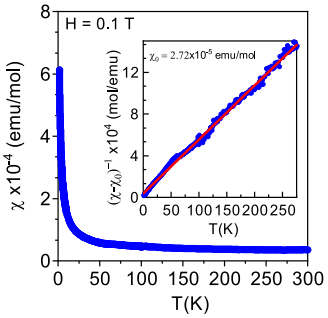

Figure 8. Temperature-dependent FC magnetic susceptibility of $LiMo_8O_{10}$ with an applied magnetic field of 0.1 T. Inset shows the plot of $(\chi - \chi_o)^{-1}$ vs T. The red line is the straight-line fit to the data.

corrected for a small diamagnetic contribution (χ_o = 2.72 × 10^{-5} emu/mol) is almost linear in the entire temperature range below 275 K as depicted in the inset of Figure 8. Fitting the data between 70 and 250 K with the modified Curie–Weiss law, $\chi = \chi_o + C/(T - \theta_w)$, yields the Weiss temperature of θ_w = −10 K, and the effective magnetic moment (μ_{eff} = 0.12 μ_B/f.u) is given by $\sqrt{8C}$, where C is the Curie constant. The obtained values of the χ_o and C are close to those in $Rb_{1.5}Mo_8O_{16}$.[35] The absence of magnetic ordering of Mo ions in $LiMo_8O_{10}$ has also been observed in related compounds with strong Mo–Mo bonding, such as $R_4Mo_4O_{11}$ (R = Y, Nd, and Sm-Tm),[12] $R_4Mo_{18}O_{32}$ (R = Y, Gd, Tb, and Ho),[36] and $Ba_3Mo_{18}O_{28}$.[37]

The temperature-dependent resistivity measurement of $LiMo_8O_{10}$ was performed on a dense pellet that was prepared at 400 °C and 4 GPa. At 300 K, the resistivity (ρ_{300}) is 0.0017 Ω•m, and it increases slowly to 0.019 Ω•m at 75 K and 0.048 Ω•m at 50 K, but starts increasing exponentially below 50 K and reaches 0.74 Ω•m at 1.8 K (Figure 9). Compared to the

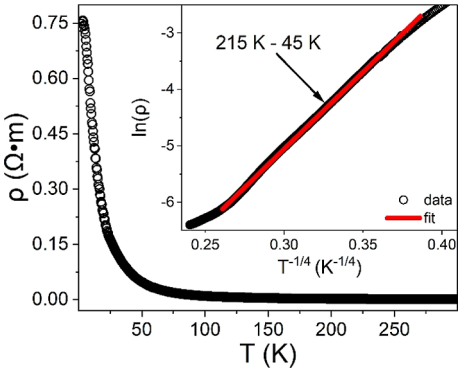

Figure 9. Temperature-dependent resistivity of $LiMo_8O_{10}$ from 300 to 1.8 K with the plot of $\ln(\rho)$ vs $T^{-1/4}$ (inset).

resistivity at 300 K, the resistivity at 1.8 K increases by a factor ($\rho_{1.8}/\rho_{300}$) of 435, which is a rare and exponential change. $Li_{0.9}Mo_6O_{17}$ also exhibits an exponential increase below ~24 K, but with a relatively small $\rho_{1.8}/\rho_{300}$ (~5) ratio.[4] This compound undergoes a superconducting state below 1.8 K.[4] The abnormal increase of resistivity of $LiMo_8O_{10}$ below 50 K requires further study to understand whether this is a simple insulator (semiconductor) or it also becomes superconducting at lower temperatures as observed in $Li_{0.9}Mo_6O_{17}$. The decreasing resistivity at high temperatures may be due to the localized carrier hopping amongst the nearest neighbor localized states. The resistivity data can be described with the Mott's variable range hopping conduction mechanism for three-dimensional conductance in the temperature ranges of 215–45 K with equation $\rho = \rho_o \exp[(T_o/T)^{1/4}]$,[38] where the preexponential factor (ρ_o) is the temperature-dependent resistivity parameter, and T_0 is the characteristic temperature, which is associated with the electronic density of states (DOS) at the Fermi level and the localization length of the carrier.

The semiconducting behavior is in contrast to the expected metallic behavior based on the strong infinite Mo–Mo bonding, which has been observed in AMo_4O_6 (A = Na and In) and $Mn_{1.5}Mo_8O_{11}$ compounds with similar edge-sharing Mo_6 octahedra feature.[9,14,15] However, the metal-to-insulator transition occurs at 118–120 and 50 K for KMo_4O_6 and $SnMo_4O_6$, respectively.[8,16,17] $R_4Mo_{18}O_{32}$ (R = Y and Gd–Yb) with Mo_2, Mo_4, and Mo_6 clusters also shows a metal-to-insulator transition in the range of 70–120 K.[36] The semiconducting behavior is also reasonable considering that there are Mo–O–Mo bonding between chains and O–Li–O bonding between layers in addition to strong Mo–Mo bonding within the infinite chains of Mo_4O_5 clusters. The semiconducting behavior has also been reported in $R_4Mo_4O_{11}$ (R = Y, Nd, and Sm-Tm) with infinite edge-sharing Mo_6 octahedra;[12] $Ba_3Mo_{18}O_{28}$ containing four edge-sharing Mo_6 octahedra;[37] and $Ca_{5.45}Mo_{18}O_{32}$ featuring Mo, Mo_2, and Mo_4 clusters chains.[15]

The field-dependent magnetoresistance (MR) of $LiMo_8O_{10}$ was measured between 2 and 30 K (Figure 10). The MR is

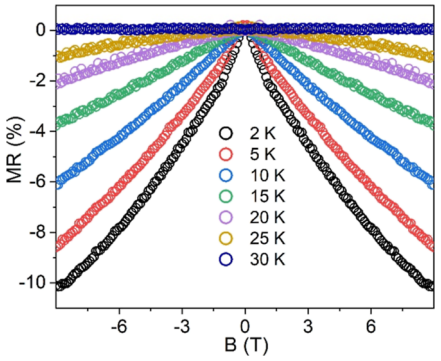

Figure 10. Field-dependent MR of $LiMo_8O_{10}$ measured between 2 and 30 K.

calculated with the definition MR = $[(\rho_B - \rho_{0T})/\rho_{0T}] \times 100\%$, where ρ_B and ρ_{0T} are the resistivities measured with applied magnetic fields B and B = 0 T, respectively. At 2 K, the MR shows negative values, and the absolute value starts increasing with increasing magnetic field and reaches the maximum value of 10.2% at 9 T. A similar negative MR trend remains between 2 and 25 K, and the magnitude decreases as the temperature increases. This is the first example of negative MR among the ternary molybdenum oxides with infinite Mo_6 octahedra. The negative MR at lower temperatures is intriguing, especially as it appears in the paramagnetic state. Usually, the MR is positive in a nonmagnetic material. In magnetic materials, the negative MR usually appears due to suppression of the spin fluctuation by the external magnetic field, and the effect becomes maximum close to the magnetic transition temperature. The negative MR in $LiMo_8O_{10}$, thus, may be an indication that

https://doi.org/10.1021/acs.inorgchem.2c01917
Inorg. Chem. XXXX, XXX, XXX–XXX

there is a magnetic ordering just below 1.8 K (the lowest temperature we could measure), or that this material has a strong spin fluctuation that is suppressing the magnetic ordering. What makes it more interesting is that a similar negative MR has been reported in $Li_{0.9}Mo_6O_{17}$ (for magnetic field applied along the crystallographic *b* axis) just above the superconductivity transition temperature at 1.8 K,[4] which has been attributed to the suppression of the fluctuations associated with the nearby superconductivity by the magnetic field. Thus, it is also likely that $LiMo_8O_{10}$ becomes a superconductor at lower temperatures and requires further study.

The temperature-dependent heat capacity (C_P) measurement was conducted on a pellet from 1.8 to 80 K. The absence of an anomaly in the C_P versus T plot suggests that there is no long-range magnetic ordering (Figure 11). The specific heat,

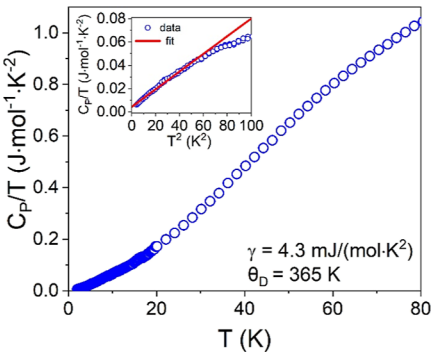

Figure 11. Heat capacity of $LiMo_8O_{10}$ measured from 1.8 to 80 K, and the low-temperature range fitted with the modified Debye model $C_P/T = \gamma + \beta T^2$ (inset).

$C_P = \gamma T + \beta T$,[3] is the sum of electron ($C_e = \gamma T$) and lattice ($C_l = \beta T^3$) specific heat. The low-temperature range (1.8 to 7 K) can be fitted with the modified Debye model $C_P/T = \gamma + \beta T^2$, which yields the electronic specific heat coefficient (Sommerfeld coefficient), $\gamma = 4.3$ mJ/(mol•K^2), and coefficient $\beta = 0.76$ mJ/(mol•K^4). The Sommerfeld constant $\gamma = \pi^2 k_B^2 N(E_F)/3$, where k_B is Boltzmann constant (1.380649 J/K, or 8.61733×10^{-5} eV/K), is proportional to the total DOS at the Fermi level, $N(E_F)$. Based on the obtained $\gamma = 4.3$ mJ/(mol•K^2), the $N(E_F)$ is calculated to be 1.8 states/eV•unit cell. The coefficient β is associated with the Debye temperature (θ_D) as $\theta_D^3 = 12\pi^4 Rn/(5\beta)$, where $R = 8.314$ J/(mol•K) and $n = 19$ (number of atoms per formula unit), and the calculated θ_D is equal to 365 K.

Electronic Structure. DFT calculations were performed to obtain the DOS of nonmagnetic $LiMo_8O_{10}$, and the results are shown in Figure 12. In the crystal structure, Mo1 and Mo2 have the coordination number of 4, while Mo3 and Mo4 have the coordination number of 5 with O atoms. Due to the different geometries, four different Mo atoms are grouped into two: Mo1 + Mo2 and Mo3 + Mo4, and the two show different 4d partial DOS, as shown in Figure 12. The computed DOS shows a metallic phase, which is opposite to the observed semiconducting behavior in the experiment (see Figure 9). Note that the forbidden energy window is realized above the Fermi level, from ~0.2 to ~0.5 eV in the computed DOS. Furthermore, introducing magnetism such as ferro-, ferri-, and antiferromagnetism does not open the bandgap in the DFT calculations. This discrepancy may be related to the drawback

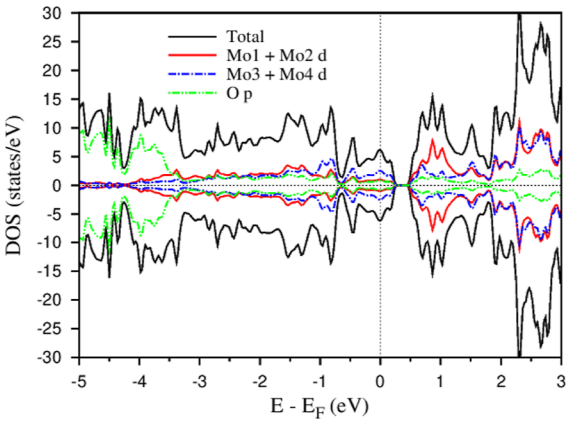

Figure 12. DOS of nonmagnetic $LiMo_8O_{10}$ with the polar space group $Cmc2_1$.

of DFT calculations as they are well known to underestimate the bandgap. Several methods like hybrid functional, modified Becke-Johnson (mBJ) exchange potential, and DFT plus dynamical mean-field theory (DFT + DMFT) were employed, but all of them were unsuccessful in giving the bandgap in this system. Other methods beyond the standard DFT framework are necessary to investigate the insulating phase of $LiMo_8O_{10}$, which remain for future work.

CONCLUSIONS

Polycrystalline $LiMo_8O_{10}$ was synthesized by annealing starting materials Li_2MoO_4, MoO_3, and Mo at 1380 °C for 48 h using a Mo crucible. The polar crystal structure featuring edge-sharing Mo_6 octahedra chains was confirmed with the Rietveld refinement of room-temperature neutron powder diffraction data. The tetrahedral environment of Li atoms in the crystal structure was confirmed by the $^7Li/^6Li$ solid-state NMR. The valence state of Mo was consistent with the formal Mo valence state according to the XANES of the Mo-L_3 edge. Resistivity measurement of $LiMo_8O_{10}$ indicates that this compound is not metallic as expected from the strong Mo−Mo bonding in the crystal structure. $LiMo_8O_{10}$ shows an interesting increase in resistivity at lower temperatures with the ratio of $\rho_{1.8}/\rho_{300}$ equal to 435, which is not observed in similar compounds with edge-sharing Mo_6 octahedra feature. Isothermal field-dependent magnetoresistance measurements at 2 K also reveal a negative magnetoresistance of 10.1% at 9 T. The study of $LiMo_8O_{10}$ provides valuable guidance for the study of isostructural $ZnMo_8O_{10}$ containing a more reduced Mo in the crystal structure, which will be carried out in the future.

ASSOCIATED CONTENT

Supporting Information

The Supporting Information is available free of charge at https://pubs.acs.org/doi/10.1021/acs.inorgchem.2c01917.

Laboratory X-ray powder diffraction pattern of $LiMo_8O_{10}$ (PDF)

AUTHOR INFORMATION

Corresponding Authors

Patrick Gougeon − *Sciences Chimiques de Rennes, UMR 6226 CNRS—INSA—Université de Rennes 1, Rennes 35042, France*; orcid.org/0000-0003-4778-5581; Email: patrick.gougeon@univ-rennes1.fr

https://doi.org/10.1021/acs.inorgchem.2c01917
Inorg. Chem. XXXX, XXX, XXX−XXX

Xiaoyan Tan − *Department of Chemistry and Biochemistry, George Mason University, Fairfax, Virginia 22030, United States;* orcid.org/0000-0002-1742-8252; Email: xtan6@gmu.edu

Authors

Zachary T. Messegee − *Department of Chemistry and Biochemistry, George Mason University, Fairfax, Virginia 22030, United States;* orcid.org/0000-0001-9702-580X

Philippe Gall − *Sciences Chimiques de Rennes, UMR 6226 CNRS—INSA—Université de Rennes 1, Rennes 35042, France*

Hari Bhandari − *Department of Physics and Astronomy and Quantum Science and Engineering Center, George Mason University, Fairfax, Virginia 22030, United States*

Peter E. Siegfried − *Department of Physics and Astronomy and Quantum Science and Engineering Center, George Mason University, Fairfax, Virginia 22030, United States;* orcid.org/0000-0002-0145-2899

Chang-Jong Kang − *Department of Physics, Chungnam National University, Daejeon 34134, Republic of Korea; Institute of Quantum Systems, Chungnam National University, Daejeon 34134, Republic of Korea;* orcid.org/0000-0003-2895-4888

Benjamin Chen − *Department of Chemistry and Biochemistry, Florida State University, Tallahassee, Florida 32306, United States*

Carl R. Conti, III − *Department of Chemistry and Biochemistry, Florida State University, Tallahassee, Florida 32306, United States*

Banghao Chen − *Department of Chemistry and Biochemistry, Florida State University, Tallahassee, Florida 32306, United States*

Mark Croft − *Department of Physics and Astronomy, Rutgers, The State University of New Jersey, Piscataway, New Jersey 08854, United States*

Qiang Zhang − *Neutron Scattering Division, Oak Ridge National Laboratory, Oak Ridge, Tennessee 37831, United States;* orcid.org/0000-0003-0389-7039

Syed N. Qadri − *U.S. Naval Research Laboratory, Washington, District of Columbia 20375, United States*

Joseph Prestigiacomo − *U.S. Naval Research Laboratory, Washington, District of Columbia 20375, United States;* orcid.org/0000-0001-5274-8836

Nirmal J. Ghimire − *Department of Physics and Astronomy and Quantum Science and Engineering Center, George Mason University, Fairfax, Virginia 22030, United States;* orcid.org/0000-0002-8474-4968

Complete contact information is available at: https://pubs.acs.org/10.1021/acs.inorgchem.2c01917

Author Contributions

[††]Z.T.M. and P.G. contributed equally.

Notes

The authors declare no competing financial interest.

■ ACKNOWLEDGMENTS

C.M.S. and X.T. were supported by start-up funding from George Mason University. C.-J.K. was supported by the NRF grant (NRF-2022R1C1C1008200). N.J.G. acknowledges the support from the National Science Foundation (NSF) CAREER award DMR- 2143903. Transport measurements were supported by the U.S. Department of Energy, Office of Science, Basic Energy Sciences, Materials Science and Engineering Division. The XANES was performed at NSLS-II beamline 7-ID-2 SST-2, under the expert guidance of Conan Weiland (NIST). The National Synchrotron Light Source II (NSLS-II) is a U.S. Department of Energy (DOE) Office of Science User Facility operated for the DOE Office of Science by Brookhaven National Laboratory under Contract no DE-SC0012704. This work used resources at the Spallation Neutron Source, DOE Office of Science Facilities operated by the Oak Ridge National Laboratory. We thank Dr. David Walker at Columbia University for preparing the dense pellet with the Walker-type high-pressure press.

■ REFERENCES

(1) Greenblatt, M.; Ramanujachary, K. V.; McCarroll, W. H.; Neifeld, R.; Waszczak, J. V. Quasi-Two-Dimensional Electronic Properties of the Sodium Molybdenum Bronze, $Na_{0.9}Mo_6O_{17}$. *J. Solid State Chem.* **1985**, *59*, 149−154.

(2) Pouget, J. P.; Kagoshima, S.; Schlenker, C.; Marcus, J. Evidence for a Peierls Transition in the Blue Bronzes $K_{0.30}MoO_3$ and $Rb_{0.30}MoO_3$. *J. Phys. Lett.* **1983**, *44*, 113−120.

(3) Degiorgi, L.; Wachter, P.; Greenblatt, M.; McCarroll, W. H.; Ramanujachary, K. V.; Marcus, J.; Schlenker, C. Optical Investigation of Quasi-One- and Two-Dimensional Systems $A_{0.9}Mo_6O_{17}$ (A = Li, K, and Na). *Phys. Rev. B: Condens. Matter Mater. Phys.* **1988**, *38*, 5821−5826.

(4) Chen, H.; Ying, J. J.; Xie, Y. L.; Wu, G.; Wu, T.; Chen, X. H. Magnetotransport Properties in Purple Bronze $Li_{0.9}Mo_6O_{17}$ Single Crystal. *Epl* **2010**, *89*, 67010.

(5) Torardi, C. C.; McCarley, R. E. Sodium Tetramolybdenum Hexoxide ($NaMo_4O_6$). A Metallic Infinite-Chain Polymer Derived by Condensation of Octahedral Clusters. *J. Am. Chem. Soc.* **1979**, *101*, 3963−3964.

(6) McCarroll, W. H.; Ramanujachary, K. V.; Greenblatt, M.; Marsh, R. E. On the Tetragonal Forms of KMo_4O_6. *J. Solid State Chem.* **1995**, *117*, 217−218.

(7) Schultz, P.; Simon, A.; Oeckler, O. Modulated Crystal Structure of $InMo_4O_6$. *Acta Crystallogr.* **2016**, *72*, 642−649.

(8) Dong-woon, J.; Kwang-sik, C.; Sung-jin, K. Factors Affecting the Magnitude of the Metal-Insulator Transition Temperature in AMo_4O_6 (A = K, Sn). *Bull. Korean Chem. Soc.* **2004**, *25*, 959−964.

(9) McCarley, R. E. Halide and Chalcogenide Clusters of the Early Transition Metals. *Philos. Trans. R. Soc., A* **1982**, *308*, 141−157.

(10) Hainz, M.; Boller, H. $GaMgMo_4O_7$ and $Fe_2Mo_4O_7$ - Two Low-Valent Molybdenum Oxides with a Fully Ordered $Sc_{0.75}Zn_{1.25}Mo_4O_7$ Type Structure. *J. Alloys Compd.* **2001**, *317−318*, 132−135.

(11) Lii, K. H.; McCarley, R. E.; Kim, S.; Jacobson, R. A. Synthesis and Structure of Ternary Molybdenum Oxides MMo_8O_{10} (M = Li or Zn) Having Orthogonal Nonintersecting Octahedral Cluster Chains. *J. Solid State Chem.* **1986**, *64*, 347−358.

(12) Gall, P.; Barrier, N.; Gautier, R.; Gougeon, P. S. Structural Trends, and Physical and Electronic Properties of the Reduced Molybdenum Oxides $R_4Mo_4O_{11}$ (R = Nd-Tm and Y) Containing Infinite Chains of Trans-Edge-Shared Octahedral Clusters. *Inorg. Chem.* **2002**, *41*, 2879−2885.

(13) Gall, P.; Gougeon, P. Redetermination of $Mn_{1.44}Mo_8O_{11}$: Evidence of Pairwise Distortion of Octahedral Molybdenum Chains. *Acta Crystallogr.* **2006**, *62*, i155−i157.

(14) Carlson, C. D.; Brough, L. F.; Edwards, P. A.; McCarley, R. E. Synthesis, Structure and Properties of Manganese Molybdenum Oxide ($Mn_{1.5}Mo_8O_{11}$), a Unique Structure Type among Compounds Having Infinite Chains of Trans-Edge-Shared Octahedral Cluster Units. *J. Less Common. Met.* **1989**, *156*, 325−339.

(15) McCarley, R. E.; Lii, K.-H. P. A.; Edwards, L. F.; Brough, L. F. New Extended Clusters in Ternary Molybdenum Oxides. *J. Solid State Chem.* **1985**, *57*, 17−24.

(16) Andrade, M.; Maffei, M. L.; Alves, L. M. S.; Santos, C. A. M.; Ferreira, B.; Sartori, A. F. Microstructure and Metal-Insulator Transition in Single Crystalline KMo_4O_6. *Mater. Res.* **2012**, *15*, 998−1002.
(17) Ramanujachary, K. V.; Greenblatt, M.; Jones, E. B.; McCarroll, W. H. Synthesis and Characterization of a New Modification of the Quasi-Low-Dimensional Compound Potassium Molybdate (KMo_4O_6). *J. Solid State Chem.* **1993**, *102*, 69−78.
(18) McCarley, R. E. Some Structure-Bonding Correlations in Reduced Ternary Molybdenum Oxides with Infinite Chains of Edge-Shared Octahedral Cluster Units. *Polyhedron* **1986**, *5*, 51−61.
(19) Benedek, N. A.; Birol, T. "F." M. Fundamental Mechanisms and Design Considerations for New Materials. *J. Mater. Chem. C* **2016**, *4*, 4000−4015.
(20) Kirkham, M.; Heroux, L.; Ruiz-Rodriguez, M.; Huq, A. AGES: Automated Gas Environment System for in Situ Neutron Powder Diffraction. *Rev. Sci. Instrum.* **2018**, *89*, 092904.
(21) Rodríguez-Carvajal, J. Recent Advances in Magnetic Structure Determination by Neutron Powder Diffraction. *Phys. Rev. B: Condens. Matter Mater. Phys.* **1993**, *192*, 55−69.
(22) Blaha, P. S.; Schwarz, K.; Madsen, G. K. H.; Kvasnicka, D.; Luitz, J. *WIEN2K An Augmented Plane Wave + Local Orbitals Program for Calculating Crystal Properties*; Technische Universität Wien: Wien: Austria, 2001.
(23) Brown, I. D.; Wu, K. K. Empirical Parameters for Calculating Cation-Oxygen Bond Valences. *Acta Crystallogr. Sect. B* **1976**, *32*, 1957−1959.
(24) Bart, J. C. J.; Ragani, V. Molybdenum Oxygen Bond-Strength Bond-Length Relationships. *Inorg. Chim. Acta.* **1979**, *36*, 261−265.
(25) Hughbanks, T.; Hoffmann, R. Chains of Trans-Edge-Sharing Molybdenum Octahedra: Metal-Metal Bonding in Extended Systems. *J. Am. Chem. Soc.* **1983**, *105*, 3528−3537.
(26) Wheeler, R. A.; Hoffmann, R. Trans-Edge-Sharing Molybdenum Octahedra: A Reciprocal Space Approach to Metal-Metal Bonding in Finite Chains. *J. Am. Chem. Soc.* **1988**, *110*, 7315−7325.
(27) MacKenzie, K. J. D.; Smith, M. E. *Multinuclear Solid-State NMR of Inorganic Materials*, 1st ed.; Pergamon, 2002.
(28) Zeng, Z.; Fawcett, I. D.; Greenblatt, M.; Croft, M. Large Magnetoresistance in Double Perovskite $Sr_2Cr_{1.2}Mo_{0.8}O_{6-\delta}$. *Mater. Res. Bull.* **2001**, *36*, 705−715.
(29) Veith, G. M.; Greenblatt, M.; Croft, M.; Goodenough, J. B. Synthesis and Characterization of the Oxynitride Pyrochlore - $Sm_2Mo_2O_{3.83}N_{3.17}$. *Mater. Res. Bull.* **2001**, *36*, 1521−1530.
(30) de Groot, F. M. F.; Hu, Z. W.; Lopez, M. F.; Kaindl, G.; Guillot, F.; Tronc, M. Differences between L3 and L2 X-Ray Absorption Spectra of Transition Metal Compounds. *J. Chem. Phys.* **1994**, *101*, 6570−6576.
(31) Svyazhin, A.; Nalbandyan, V.; Rovezzi, M.; Chumakova, A.; Detlefs, B.; Guda, A. A.; Santambrogio, A.; Manceau, A.; Glatzel, P. Chemical Information in the L3 X-Ray Absorption Spectra of Molybdenum Compounds by High-Energy-Resolution Detection and Density Functional Theory. *Inorg. Chem.* **2022**, *61*, 869−881.
(32) Popov, G.; Greenblatt, M.; Croft, M. Large Effects of A-Site Average Cation Size on the Properties of the Double Perovskites $Ba_{2-x}Sr_xMnReO_6$: A d^5-d^1 System. *Phys. Rev. B: Condens. Matter Mater. Phys.* **2003**, *67*, 024406.
(33) Alp, E. E.; Goodman, G. L.; Soderholm, L.; Mini, S. M.; Ramanathan, M.; Shenoy, G. K.; Bommannavar, A. S. A New Approach to Determining the Charge Distribution in Copper Compounds. *J. Phys. Condens. Matter* **1989**, *1*, 6463−6468.
(34) Croft, M.; Sills, D.; Greenblatt, M.; Lee, C.; Cheong, S.-W.; Ramanujachary, K. V.; Tran, D. Systematic Mn D-Configuration Change in t System: A Mn K-Edge XAS Study. *Phys. Rev. B: Condens. Matter Mater. Phys.* **1997**, *55*, 8726−8732.
(35) Ozawa, T.; Suzuki, I.; Sato, H. Structural, Magnetic and Electronic Transport Properties of Novel Hollandite-Type Molybdenum Oxide, $Rb_{1.5}Mo_8O_{16}$. *J. Phys. Soc. Jpn.* **2006**, *75*, 014802.
(36) Gall, P.; Gougeon, P.; Ramanujachary, K. V.; McCarroll, W. H.; Greenblatt, M. Anomalous Metal-Insulator Transitions in Reduced Molybdenum Oxides, $A_4Mo_{18}O_{32}$ (A = Ca, Y, Gd-Yb) with Mon (n = 2,4,6) Cluster Chains. *J. Solid State Chem.* **1997**, *134*, 45−51.
(37) Schimek, G. L.; Nagaki, D. A.; McCarley, R. E. Synthesis and Characterization of $Ba_3Mo_{18}O_{28}$: A Metal-Metal-Bonded Oligomer Containing Four Trans Edge-Shared Molybdenum Octahedra. *Inorg. Chem.* **1994**, *33*, 1259−1265.
(38) Mott, N. F. *Conduction in Non-Crystalline Materials*, 2nd ed.; Clarendon Press: Oxford, 1993.

https://doi.org/10.1021/acs.inorgchem.2c01917
Inorg. Chem. XXXX, XXX, XXX−XXX